ELSEVIER

Materials Science and Engineering A 437 (2006) 38–45

MATERIALS SCIENCE & ENGINEERING A

www.elsevier.com/locate/msea

A comparison of inertia friction welds in three nickel base superalloys

M. Preuss [a,*], P.J. Withers [a], G.J. Baxter [b]

[a] *School of Materials, University of Manchester, Grosvenor St., Manchester M1 7HS, UK*
[b] *Rolls-Royce plc. Derby, UK*

Received 2 July 2005; accepted 15 April 2006

Abstract

In this paper the microstructure, mechanical properties and residual stresses are compared for three inertia friction welded nickel-base superalloys. In contrast to alloy 720Li and RR1000, for Inconel 718 welding produces a precipitation free region leading to significantly reduced strength near the weld line. As a result, for alloy 720Li the hoop stresses are 1.5 times, and in RR1000 two times, higher than the tensile hoop stresses for Inconel 718. The maximum tensile weld stresses in Inconel 718 and RR1000 are yield stress limited in the weld region. That stresses significantly below the yield stress are found near the weld for alloy 720Li may be because the inferior creep properties of alloy 720Li compared to RR1000 result in stress relief during cooling after welding.

Post weld heat treatment at the standard maximum aging temperature for Inconel 718 (732 °C), relieved residual hoop stresses to below 400 MPa. To achieve a similar level of residual hoop stress, Alloy 720Li must be stress relieved at least 30 °C and RR1000 about 80 °C hotter.

Keywords: Neutron diffraction; Residual stresses; Inertia friction welding; Post weld heat treatment; Ni superalloys

1. Introduction

Inertia friction welding is a solid state welding process able to join the new generation of high volume fraction γ' nickel-base superalloys. These alloys are very difficult to fusion weld and are prone to micro-cracking as solidification takes place during welding [1,2]. Furthermore, it is recognised that inertia friction welding is better suited to mass production than electron beam welding since it does not require a vacuum during the joining process [3]. In inertia friction welding, an axis-symmetric work-piece is rotated to a specified speed and then a second, stationary, work-piece is forced into frictional engagement with the first. If the correct welding parameters are chosen, the frictional heat is sufficient to soften the two components in the weld region without introducing melting [4]. It has been shown that the heat affected zone (HAZ) can be very narrow if tubular shaped components with a wall thickness of 10–11 mm are joined together [5,6]. Due to the extreme thermo-mechanical history, the microstructure is heavily modified in the HAZ of a joint. Various studies of inertia friction welded nickel-based superalloys in the as-welded condition have shown two different types of hardness profiles in the HAZ. Alloys such as Waspaloy (25% γ') and Inconel 718 (25% γ'/γ'') generally exhibit a pronounced hardness drop, which is attributed to the absence of γ' in this region after welding [7,8]. However, alloys like N18, Astroloy, Alloy 720Li and RR1000, which contain about 50% γ', show a hardness peak in the HAZ [5,6,9]. The hardness peak is due to the large driving force for precipitation even at extremely high cooling rates. The different reprecipitation behaviours can be expected to have consequences for residual stress levels generated during joining. For example, a soft (low yield point) near weld line region in Inconel 718 will limit residual stress generation since this is where one would expect the highest tensile hoop stresses [10]. Until now, there have been no data comparing residual stress measurements of inertia friction welds from different nickel base superalloys formed under similar conditions. Some of the residual stress work reported in the open literature has been either limited to the axial direction [11,12] or failed to include the issue of stress-free lattice parameter variation across the weld line [13,14] which has been shown to be important for inertia friction welded RR1000 [10].

This paper focuses on the interplay between across-weld microstructural/mechanical property variations and residual stress generation during inertia friction welding Inconel 718, Alloy 720Li and RR1000. In view of the drive to form dissimilar welds combining these three different types of nickel-base

* Corresponding author. Tel.: +44 161 306 3601; fax: +44 161 3063586.
E-mail address: michael.preuss@manchester.ac.uk (M. Preuss).

0921-5093/$ – see front matter © 2006 Elsevier B.V. All rights reserved.
doi:10.1016/j.msea.2006.04.058

Table 1
Chemical composition (wt.% of main alloying elements, balance nickel) of Inconel 718, Alloy 720Li and RR1000

Alloy	Cr	Co	Fe	Mo	Nb	W	Al	Ti	Ta	Hf
Inconel 718	19	–	17	3.1	5.2		0.5	0.9	–	–
U720 LI	16	15	–	3.0	–	1.25	2.5	5.0	–	–
RR1000	14.35–15.15	14.0–19.0	–	4.25–5.25	–	–	2.85–3.15	3.45–4.15	1.35–2.15	0.0–1.0

superalloy it is necessary to understand the metallurgical and residual stress issues associated with each alloy. Another important aspect, given that the three alloys studied have different high temperature mechanical properties, is effective post weld stress relief. For this reason, Inconel 718, Alloy 720 and RR1000 inertia friction welds have been residual stress mapped after post weld heat treatment (PWHT) at temperatures applied typically during the aging of each alloy. The results of the residual stress measurements are presented in this paper.

2. Experimental

2.1. Material

The chemical compositions of Inconel 718, Alloy 720Li and RR1000 [15–17] are listed in Table 1. RR1000 and Alloy 720Li have a larger wt.% of Al and Ti than Inconel 718 and consequently a significantly higher volume fraction of γ' ($(Ni, Co)_3$ (Al, Ti) [2]). This affects markedly the development of microstructure. The three alloys used for this investigation came from fully heat-treated and annealed forgings. Rings with an outer diameter (OD) of 143 mm, a wall thickness of 10–11 mm and an axial length of 50 mm were machined from the forging and subsequently inertia welded at MTI, South Bend, Indiana, USA. Two welds of each alloy were available in order to study the as-welded and PWHT'd condition. The PWHT were carried out using small chamber furnaces with a temperature accuracy of ±2 °C. For the microstructural studies, samples were machined across the weld line of the joint assembly after the residual stress measurements had been completed. The samples were then sectioned for subsequent investigations.

2.2. Mechanical cross-weld testing

In order to evaluate the mechanical properties of the development inertia friction welds microhardness mapping and tensile testing in conjunction with surface strain field measurements were undertaken on samples in the as-welded condition. Microhardness testing was carried out under a load of 1 kg using a calibrated Vickers hardness indentation machine. The average indentation size was between 60 and 70 μm, giving a high spatial resolution across the weld line. With an average grain size of less than 5 μm in RR1000 [5] (powder-metallurgical alloy), each measurement sampled a sufficient number of grains. Since the base Alloy 720Li and Inconel 718 materials (cast alloys) displayed a relatively large mean grain size (10–20 μm, measured using scanning electron microscopy back scatter images), hardness indents often covered only a small number of grains leading to a significantly higher scatter in the microhardness profiles. The polished and etched samples were aligned with the indented surface perpendicular to the hoop direction. For each sample, measurements were carried out on a grid of five lines parallel to the axial direction and spaced greater than four indentations apart.

Tensile testing was carried out on cylindrical cross-weld specimens electro discharge machined (EDM) from the three welds in the as-welded condition. In order to capture the cross-weld strain variation during tensile loading, in situ surface strain field recording was carried out using a commercial electron speckle pattern interferometry (ESPI) system (Ettemeyer Q300). ESPI offers the possibility of full field and non-contact measurement of displacements and strains [18]. ESPI has sufficient strain resolution to reconstruct local stress–strain curves. This is done by continuously recording strain maps at increasing loads during tensile testing. By identifying the strain at each location as a function of applied load, it is possible to recover many stress–strain curves from a single tensile test corresponding to different positions across the weld line. From the reconstructed stress strain curves the 0.2% proof stress can be determined in a conventional manner. This technique has been recently used to record 0.2% proof stress profiles across friction welds with a spatial resolution better then 50 microns [19,20].

2.3. Microstructural studies

Since the γ' distribution is known to vary dramatically over a few millimeters from the weld line in 11 mm wall thickness inertia friction welded nickel-base Superalloys [5,6], spatial accuracy during microstructural studies is of great importance. High energy X-ray synchrotron diffraction measurements were undertaken on the ID11 beam line at the European Synchrotron Radiation Facility (ESRF) in Grenoble, France, in order to quantify the fraction of γ' across the welded region. Diffraction profiles were collected in transmission on cross-sectional slices cut from the inertia friction welded tube (as-welded condition) so as to contain the axial and radial directions and then electropolished to an average thickness of 1 mm. A monochromatic beam of 60 keV energy ($\lambda = 0.208321$ Å) was stopped down by slits to 150 μm in the axial and 3 mm in the radial direction and scanned (axially) across the weld. The high intensity of the synchrotron beam allowed accurate measurements of the (1 0 0) superlattice reflection, arising from the ordered γ' phase (LI_2 structure), where the (1 0 0) refection is systematically absent for the disordered γ matrix phase. Since γ and γ' are coherent with a simple cube–cube ([0 0 1]||[0 0 1]) relationship, by normalizing the integrated intensity of the superlattice reflection with the integrated intensity of the (2 0 0) reflection, any influence of the texture on the measurement could be elim-

inated and the obtained value related to the volume fraction of γ' [21].

2.4. Residual stress measurements

Measurements were carried out on the ENGIN and ENGIN-X time-of-flight diffractometers at the ISIS neutron spallation source, Rutherford Appleton Laboratory, UK [22]. The orientation of the specimens with respect to the neutron beam were such that the axial, radial and hoop elastic strain components could be measured across the weld cross section [14]. The sampling gauge volume was defined by the intersection of the incident and diffracted beams. Changes in the lattice parameter, a, were determined by Rietveld refinement of the spectra [23]. In each case, line scans were carried out at three different radial positions across the weld line. In view of the expected symmetry across the weld lines ($z = 0$ mm), only one half of the weld cross-sections were measured.

The strains were calculated using:

$$\varepsilon = \frac{a - c(z)a_0}{c(z)a_0} \quad (1)$$

where a_0 is the stress-free lattice parameter in the parent and $c(z)$ is the correction factor that accounts for the stress-free variation in lattice parameter arising from the chemical variation of the γ phase as a function of distance from the weld line (z). The stress-free lattice parameter in the parent was generally determined by a far field measurement. A boundary condition of the axial stress field is that the stresses between the inner and outer diameter at a constant axial position (z = const.) must balance. This condition was used to infer the variation in stress free lattice parameter as a function of distance from the weld (i.e. $c(z)$—see Eq. (1)). Previous work [10] has demonstrated that results inferred from the stress-balance criterion are in excellent agreement with direct measurements of the d_0 variation made using the biaxial $\sin^2\psi$ approach.

The corresponding axial, radial and hoop residual stress fields were calculated using:

$$\sigma_{\text{axial}} = \frac{E}{(1+\nu)(1-2\nu)}[(1-\nu)\varepsilon_{\text{axial}} + \nu(\varepsilon_{\text{radial}} + \varepsilon_{\text{hoop}})], \text{ etc.} \quad (2)$$

where E is the bulk Young's modulus, and ν the Poisson's ratio (values used for each alloy can be seen in Table 2). In order to compare the measured residual stresses to the elastic limit of the material in the HAZ, the equivalent stress for each axial position was calculated using the following equation [24]:

$$\sigma_{\text{eq}} = \sqrt{0.5((\sigma_{\text{radial}} - \sigma_{\text{axial}})^2 + (\sigma_{\text{axial}} - \sigma_{\text{hoop}})^2 + (\sigma_{\text{hoop}} - \sigma_{\text{radial}})^2)} \quad (3)$$

Table 2
Young's modulus and Poisson's ratio of the three nickel-base superalloys [31]

Alloy	Young's modulus	Poisson's ratio
Inconel 718	208	0.29
Alloy 720Li	226	0.26
RR1000	224	0.24

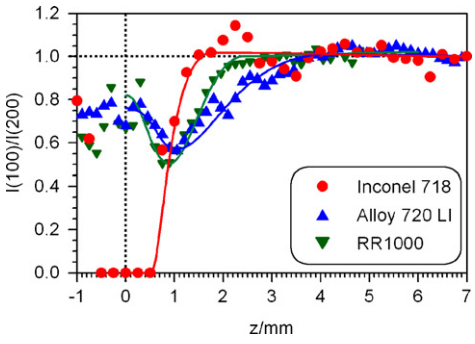

Fig. 1. The normalized integrated intensity of the γ' superlattice reflection measured on ID11 at the ESRF as a function of axial distance from the weld line (z) in the as-welded conditions. The accuracy of the data points is about ±0.04.

In this way the three-dimensional stress field was transformed into a von Mises equivalent quasi-uniaxial stress.

3. Results and discussion

3.1. Cross-weld microstructure and mechanical property variations

The mechanical properties are largely governed by the γ' distribution in precipitation strengthened nickel-base superalloys [25–27]. After standard thermomechanical treatments Alloy 720Li and RR1000 display a tri-modal γ' distribution with intergranular γ' usually in the range of 1–2 μm, secondary γ' between 150 and 250 nm and tertiary γ' typically smaller than 30 nm [5,6,25]. Inconel 718 exhibits a fine γ'/γ'' distribution (<50 nm) after the standard aging procedure [28]. The γ' distribution across an inertia friction weld can vary markedly [5,6,9]. The aim here is not to give a detailed microstructural description across the HAZ of the welds but to relate the microstructure and mechanical properties in the weld zones to the residual stress generated during the welding process. Fig. 1 summarises the overall variations in γ' distribution in the HAZ for Inconel 718, Alloy 720Li and RR1000 development inertia friction welds in the as-welded condition. It can be clearly seen that both Alloy 720Li and RR1000 display a γ' trough at around 1 mm from the weld line but that the volume fraction of γ' recovers close to the weld line. It has been demonstrated that during the welding process an increasing amount of γ' is dissolved as one approaches the weld line [5,6]. However, due to the high levels of Ti and Al in these alloys (see Table 1), the driving force for reprecipitation during fast cooling seems to be large enough to prevent any further drop in intensity within 1 mm of the weld. In [5] and [6] it was shown that at 1 mm from the weld line only partial dissolution of γ' had taken place during welding. Therefore, it can be assumed that the driving force for reprecipitation is larger at the weld line than 1 mm from it, which

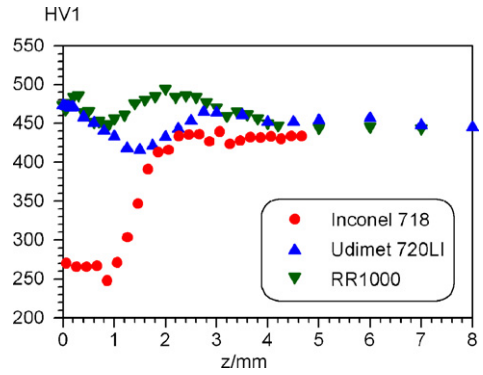

Fig. 2. Vickers hardness profiles of Inconel 718, Alloy 720Li and RR1000 inertia friction welds in the as-welded condition as a function of axial distance from the weld line ($z=0$) measured at the mid-wall thickness. The accuracy of the hardness values inferred is about ±5 HV1 for RR1000 and about 10 HV1 for Inconel 718 and Alloy 720Li. However, the smoothness of the profiles suggests a higher accuracy.

could explain the intensity trough for Alloy 720Li and RR1000 observed in Fig. 1. The high level of γ' close to the weld line in Alloy 720Li and RR1000 is reflected in relatively high Vickers hardness values (Fig. 2) and 0.2% proof stresses (Fig. 3) in this region. It is noteworthy that for RR1000 the γ' depleted zone is smaller than for Alloy 720Li with the normalised intensity value reaching the value for the parent at about 2 mm from the weld line for RR1000 compared to about 4 mm in the case of Alloy 720Li (Fig. 1). Between 1 and 3 mm from the weld line RR1000 displays generally a higher strength than Alloy 720Li. Fig. 1 might suggest that the lower strength of Alloy 720Li compared to RR1000 in this region is due to a slightly more depleted γ' region in the HAZ of Alloy 720Li. In general the microhardness profiles are in very good agreement with the 0.2% proof stress profiles.

In contrast to the two highly alloyed nickel-base superalloys, the normalised intensity of the (1 0 0) reflection drops to zero close to the weld line in Inconel 718. This indicates that reprecipitation does not take place during fast cooling. This results in a very soft region close to the weld line in the as-welded condition within 1.5 mm of the weld (Figs. 2 and 3). For Inconel 718 a yield stress of only 550 MPa was recorded in the weld zone, about half that generally recorded for the alloy [15]. As a result the cross-

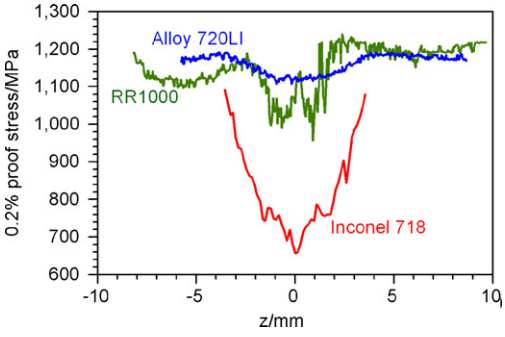

Fig. 3. A 0.2% proof stress profiles of inertia Inconel 718, Alloy 720Li and RR1000 inertia friction welds in the as-welded condition as a function of axial distance from the weld line ($z=0$). The average accuracy of the 0.2% proof stress determination varied between 10 and 50 MPa.

weld sample failed before the proof stress was achieved outside the γ'/γ'' depleted zone. In view of the differences in Fig. 3 one would expect large differences in the capability to sustain large residual stresses in the weld zone for Inconel 718 as compared with the other two alloys.

3.2. Variation of the stress-free lattice parameter

The stress free lattice parameter can be a sensitive indicator of changes in solute concentration. Fig. 4 plots the variation of the stress-free lattice parameter as derived by imposing the axial stress balance criterion. All three superalloys exhibit a significant variation of the stress-free lattice parameter ($=a_o c(z)$) in the HAZ with the stress-free lattice parameter larger than in the base material. As described above, the HAZ of inertia friction welded nickel base superalloys is characterised by changes in the amount of dissolved γ'. This results in an increased level of Ti and Al alloying elements being forced into the γ matrix widening the lattice spacing. Even though the correction factor seems to be small, if unaccounted for its impact on the residual stress field in the vicinity of the weld line would be significant. For instance failure to correct the stress-free lattice spacing at the weld line would lead to an error in the stress in the hoop direction of around +600 MPa for each alloy. It is interesting to note that the correction factors at the weld line for the three inertia friction alloys are very similar. This could indicate that for a given cooling rate the lattice parameter cannot be increased beyond a certain point. In the case of Inconel 718, the increase of the lattice parameter is sufficient to keep the γ' forming alloying elements in solution during cooling at the end of the welding process. On the other hand in Alloy 720Li and RR1000, the same expansion of the lattice is not sufficient to keep all γ' forming alloying elements in solution resulting in a reprecipitation of γ'. It should also be noted in Fig. 4 that after PWHT none of the three inertia welds display significant variations in stress-free

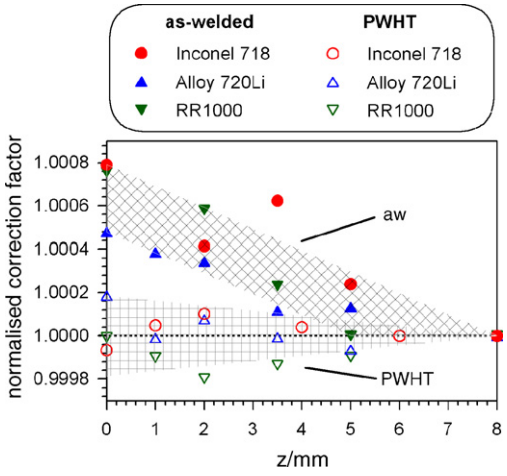

Fig. 4. Correction factor $c(z)$ calculated on the basis of imposing stress balance on the axial measurements for as-welded and PWHT'd condition for the three inertia friction welded nickel-base superalloys. The values have been normalized by the correction factor at $z=8$ mm for better comparison. The hashed areas represent the typical range for the correction factors of the as-welded and PWHT'd conditions.

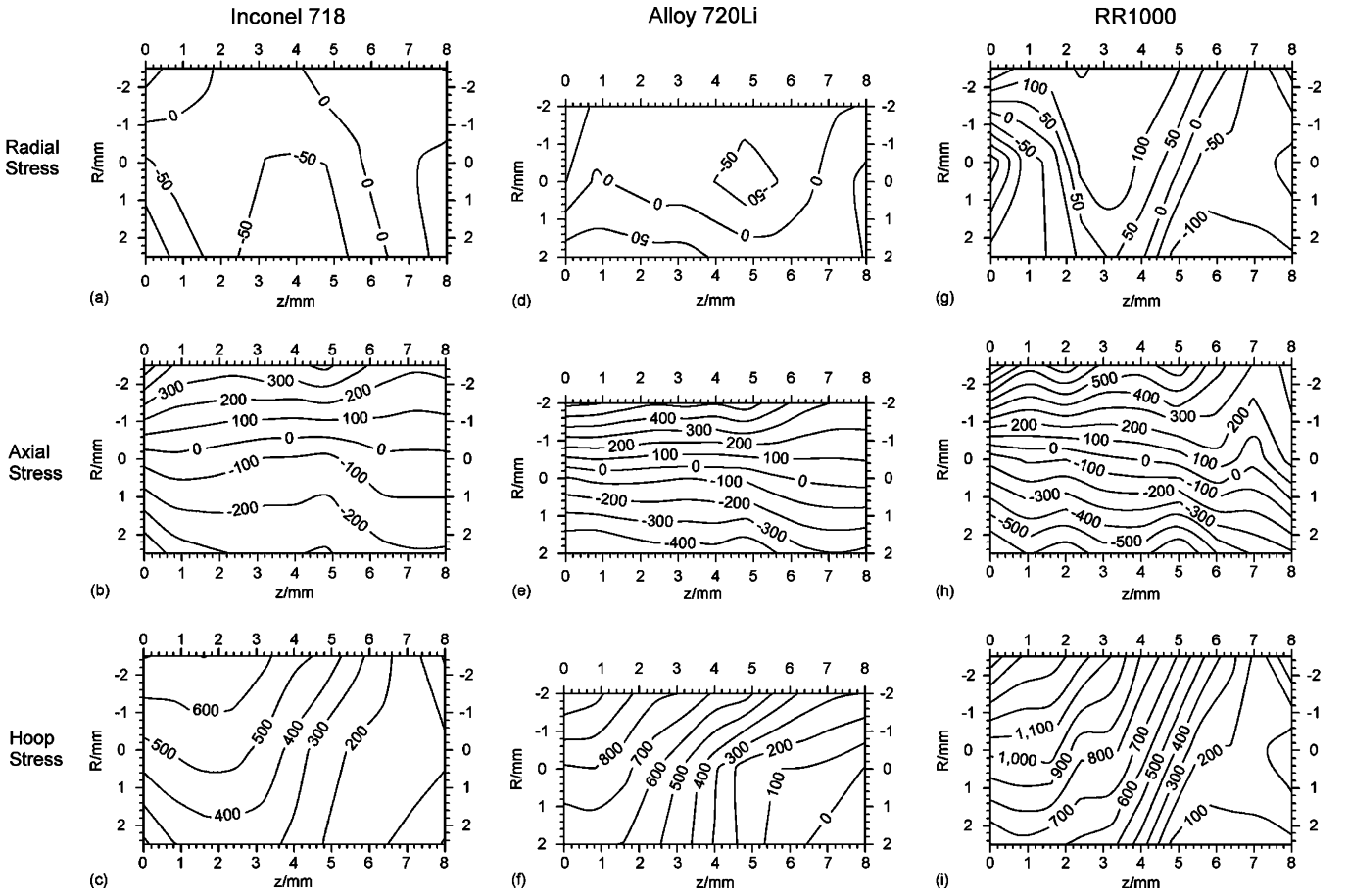

Fig. 5. Contour plots of the residual stress fields in inertia friction welded Inconel 718 (a–c), Alloy 720Li (d–f) and RR1000 (g–i) in the as-welded condition. Typical accuracy of the stress data is about ±60 MPa.

lattice parameter. This can be interpreted as an indication that γ' has fully reprecipitated during PWHT.

3.3. Residual stresses in the as-welded condition

Given that the stress-free lattice parameter has been obtained as a function of position from the welds, the residual elastic strain and stress distributions in the as-welded and PWHT'd samples can be calculated. Fig. 5a–i show the contour plots of the radial, axial and hoop stresses for Inconel 718, Alloy 720Li and RR1000 in the as-welded conditions. As one would expect, the radial stresses are small in all the welds, not exceeding 150 MPa (Fig. 5a, d and g). In contrast the axial stresses are of substantial nature displaying characteristic elastic bending profiles with tensile stresses towards the inner (R negative) and compressive stresses towards the outer (R positive) diameter (Fig. 5b, e and h). The maximum axial tensile and compressive stresses observed are about ±350 MPa in Inconel 718, ±450 MPa in Alloy 720Li and ±600 MPa in RR1000. Similar bending stress levels have been observed in finite element predictions of the residual stresses generated during inertia friction welding of RR1000 [29]. The bending moment is most likely the product of a tourniquet effect from the dominant hoop stresses [30], which varies from the inner to the outer diameter with the most concerning tensile stresses close to the inner diameter (Fig. 5c, f and i). The largest stresses are found in the hoop direction with maximum tensile hoop stresses of about 700 MPa in Inconel 718, 1000 MPa in Alloy 720Li and 1500 MPa in RR1000. The equivalent stress defined in Eq. (3) reduces the three-dimensional stress tensor to a representative uniaxial stress level. Fig. 6a displays the calculated equivalent stress profiles for all three development inertia friction welds in the as-welded condition. When comparing Figs. 3 and 6 one might expect that the equivalent stresses should at all points be less than or equal to the 0.2% yield stress. It is interesting to note that in the case of Inconel 718 the maximum tensile stresses are observed not at the weld line (as it is in Alloy 720Li an RR1000) but at 2 mm from the weld line. Fig. 6b plots the equivalent stresses from Fig. 6a divided by the 0.2% proof stresses from Fig. 3. For RR1000 the equivalent stress at the weld line slightly exceeds the local 0.2% proof stress evident in a value larger than one. This suggests that for RR1000 the stresses close to the weld are limited by the local yield stress. In contrast the stresses near the weld line in Inconel 718 and Alloy 720Li are not close to the local yield stress, which can be seen in values well below 1. The reason for the proportionately lower hoop stresses levels in Inconel 718 Alloy 720Li compared to RR1000 is currently unclear. It might be related to inferior short timescale creep properties of Inconel 718 and Alloy 720Li

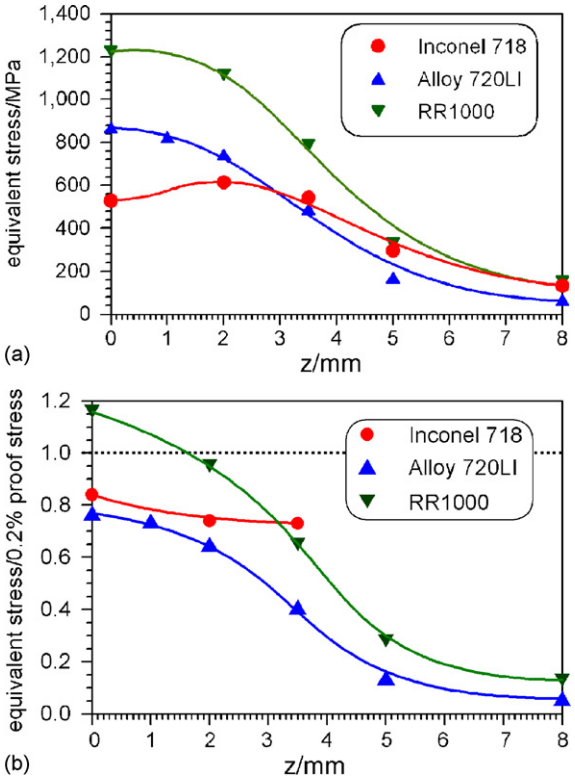

Fig. 6. (a) Profiles of the equivalent stress (Eq. (3)) and (b) profiles of the equivalent stress divided by the 0.2% proof stress (Fig. 3) with distance from the weld line for Inconel 718, Alloy 720Li and RR1000 in the as-welded condition.

compared to RR1000 allowing the misfit strains to relax during cooling rather than rise to reach the yield stress. This is currently being investigated by complementary measurements aimed at determining the yielding behaviour as a function of strain rate and temperature.

It is also noteworthy that for RR1000 further residual stress measurements were made on rings welded under a range of inertia welding conditions. The stresses were largely insensitive to the welding conditions being close to the local yield stress in all cases.

3.4. Residual stresses after post weld heat treatment

Fig. 7 plots contour maps of the radial, axial and hoop stresses for Inconel 718, Alloy 720Li and RR1000 in the PWHT'd condition. It is important to remember that the PWHT temperatures were different for the three superalloys. The stress relief temperature was tuned to the particular alloy being 732 °C (Inconel 718), 760 °C (Alloy 720Li) and 810 °C (RR1000). Just as for the as-welded condition the radial stresses were close to zero after PWHT (Fig. 7a, d and g). The axial stresses were significantly reduced in all three alloys by the PWHT with axial bending stresses relieved essentially to zero in Inconel 718 (Fig. 7b) and not exceeding 100 MPa in Alloy 720Li (Fig. 7e) and RR1000 (Fig. 7h). After PWHT the largest tensile stresses are still found in the hoop direction being around 400 MPa in Inconel 718 (Fig. 7c), 500 MPa in Alloy 720Li (Fig. 7f) and 400 MPa in

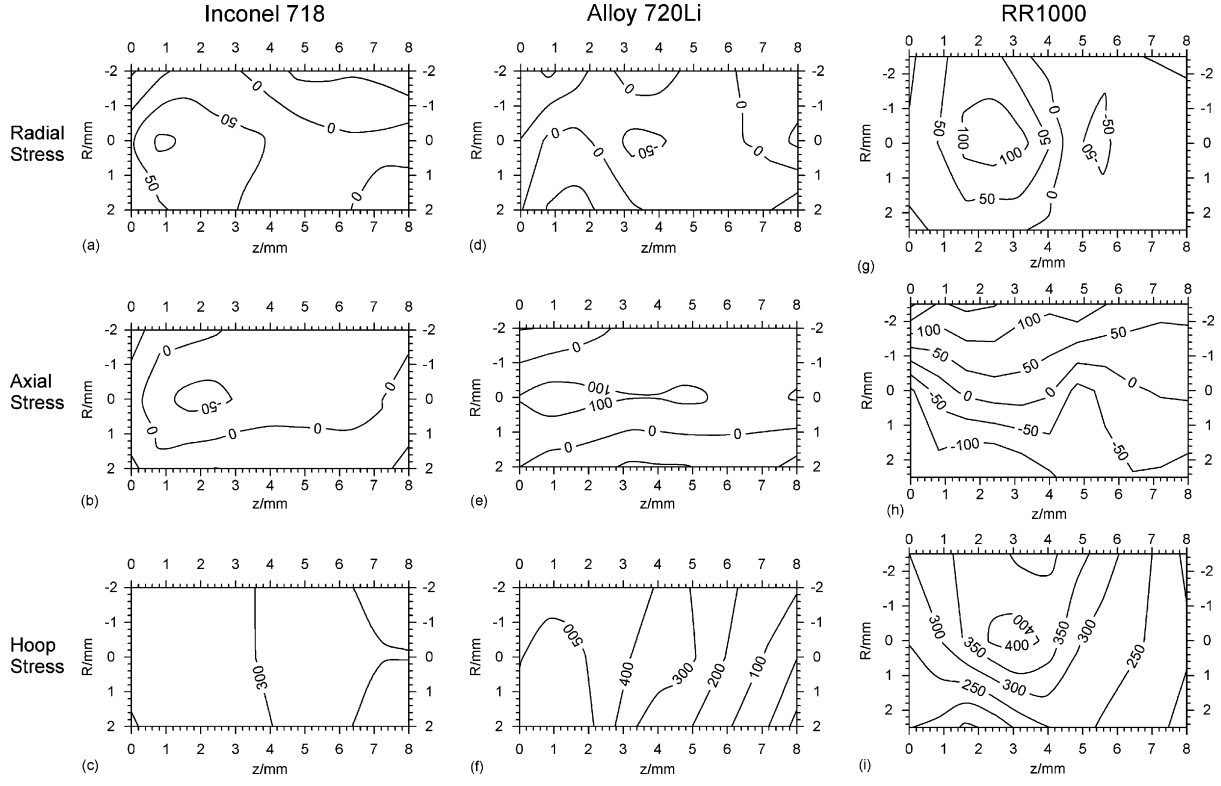

Fig. 7. Contour plots of the residual stress fields in inertia friction welded Inconel 718 (a–c), Alloy 720Li (d–f) and RR1000 (g–i) in the PWHT'd condition. Typical accuracy of the stress data is about ±60 MPa.

RR1000 (Fig. 7h). The extensive level of residual stress relief observed for RR1000 is due to the relatively high heat treatment temperature. Unlike the temperatures chosen for Alloy 720Li and Inconel 718 it slightly exceeds the aging temperatures considered typical for this alloy. Unsurprisingly, Fig. 7 demonstrates that the PWHT temperature must be chosen in line with the operating and aging temperature of the alloy.

4. Summary and conclusions

Residual stress distributions have been mapped in as-welded and PWHT'd Inconel 718, Alloy 720Li and RR1000 development inertia friction welds. Whereas Inconel 718 is a high strength nickel-base superalloy containing a volume fraction of about 25% γ' and γ'', Alloy 720Li and RR1000 have significantly higher levels of Ti and Al giving a γ' volume fraction of almost 50%, when fully annealed.

In addition, the variation of γ' distribution and mechanical properties across the weld-line have been characterised using synchrotron radiation, microhardness testing and tensile testing in conjunction with electron speckle pattern interferometry surface strain mapping. The conclusions can be summarized as follows:

1. For Inconel 718 γ' completely dissolves in the vicinity of the weld line during inertia rotational friction welding and does not reprecipitate during cooling. This results in a soft weld zone with a proof stress of about 625 MPa at the weld line.
2. In contrast, for Alloy 720Li and RR1000 close to the weld line dissolved γ' largely reprecipitates during cooling. This is most likely due to the high levels of Al and Ti found in these high γ' vol.% nickel-base superalloys. The reprecipitation of most of the γ' (as fine precipitates) results in relatively high strength levels in the HAZ of both alloys.
3. Large axial and hoop stresses are found near the welds in the as-welded condition. In each case the largest tensile stresses arise in the hoop direction either near the weld line (Inconel 718) or at the weld line (Alloy 720Li and RR1000) close to the inner diameter of the rings. The axial stress fields display a significant bending moment in all three cases.
4. Although similar welding parameters were used to join the three alloys, the axial and hoop stresses were very different for the three alloys. The largest residual tensile stresses were 700 MPa in Inconel 718, 1000 MPa in Alloy 720Li and 1500 MPa in RR1000.
5. When comparing the equivalent residual stresses with the cross-weld 0.2% proof stress profiles it seems that the residual stresses generated during welding are limited by the yield point at the weld line in RR1000 but not in Inconel 718 and Alloy 720Li. Stress relief during cooling might be more significant in Inconel 718 and Alloy 720Li than in RR1000 due inferior high strain rate creep properties in these alloys. This is currently being investigated by using a finite element approach to predict the residual stress development in inertia friction welds.
6. By using the standard maximum aging temperature for Inconel 718 ($T = 723\,^{\circ}C$), residual hoop stresses can be relieved to below 400 MPa. In order to achieve similar levels of residual hoop stress, Alloy 720Li and RR1000 must be PWHT'd at temperature 30 and 80 °C hotter, respectively, reflecting their higher aging and operating temperatures.

Acknowledgements

The authors would like to thank Drs. M.R. Daymond and J. Dann (ISIS, ENGIN-X) and Drs. J. Wright and G. Vaughan (ESRF, ID11) for experimental assistance. These experiments were performed under the EPSRC project GR/M68704 and are financially supported by Rolls-Royce plc. PJW acknowledges support of a Royal Society-Wolfson Award.

References

[1] J.K. Tien, T. Caulfield (Eds.), Superalloys, Supercomposites and Superceramics, Academic Press Inc. Ltd., London, 1989, pp. 142–143.
[2] C.T. Sims, W.C. Hagel (Eds.), The Superalloys, John Wiley, New York, 1972, pp. 509–532.
[3] R. Spinat, Y. Honnorat, in: W. Betz, et al. (Eds.), High Temperature Alloys for Gas Turbines and Other Applications, D. Reidel, Dordrecht, 1986, pp. 151–157.
[4] K.K. Wang, Welding Res. Council Bull. 204 (1975) 1–22.
[5] M. Preuss, J.W.L. Pang, P.J. Withers, G.J. Baxter, Metall. Mater. Trans. 33A (2002) 3115–3125.
[6] M. Preuss, J. Quinta da Fonseca, I. Kyriakoglou, P.J. Withers, G.J. Baxter, in: K.A. Green (Ed.), Superalloy 2004, TMS, 10th Int. Symposium, Seven Springs, Champion, PA, 2004, pp. 477–484.
[7] P. Adam, Welding of high strength gas turbine alloys, Applied Science Publisher Ltd., 1978, pp. 737–768.
[8] K.G. Schmitt-Thomas, P. Adam, H. Meisel, R. Siede, Z. Mettalkde 73 (1982) 558–565.
[9] J.P. Ferte, J. Phys. IV 3 (1993) 1019–1027.
[10] M. Preuss, J.W.L. Pang, P.J. Withers, G.J. Baxter, Metall. Mater. Trans. 33A (2002) 3127–3134.
[11] H.G. Priesmeyer, J. Schroeder, in: H. Fujiwara, T. Abe, K. Tanaka (Eds.), Residual Stresses—III: Science and Technology, Elsevier Applied Science, London, 1992, pp. 253–258.
[12] M.Es. Abdel Moniem, S.M. Serag, A.A. Nasses, A.A. Moustafa, Wear 70 (1981) 227–241.
[13] H.U. Baron, Third International Conference on Welding in Aerospace Industry, German Welding Society, Essen, 1993, pp. 114–117.
[14] J.W.L. Pang, M. Preuss, P.J. Withers, G.J. Baxter, Sixth Conference on Residual Stresses (ICRS-6), IOM Communication, London, 2000, pp. 1415–1421.
[15] D.F. Paulonis, J.M. Oblak, D.S. Duvall, Trans. ASM 62 (1969) 611–622.
[16] S.J. Hessell, et al., Nickel Alloy for Turbine Engine Components, US Patent Number 5,897,718, 27 April 1999.
[17] C.T. Sims, N.S. Stoloff, W.C. Hagel (Eds.), Superalloys II, High Temperature Materials for Aerospace and Industrial Power, John Wiley & Sons Inc., New York, 1987, pp. 221–226.
[18] A.J. Moore, J.R. Tyrer, Opt. Lasers Eng. 24 (5–6) (1996) 381–402.
[19] M.J. Peel, M. Preuss, A. Steuwer, M. Turski, P.J. Withers, Proc. 6th Conf. on Trends in Welding Research USA, 2003, pp. 273–278.
[20] J. Quinta da Fonseca, P. Ryan, M. Preuss, P.J. Withers, Proceedings of Advances in Experimental Mechanics, M. Lucas (Ed.), in: Applied Mechanics and Materials, vols. 1–2, 2004, pp. 147–152.
[21] A. Royer, P. Bastie, M. Véron, Acta. Mater. 46 (1998) 5357–5368.
[22] J.A. Dann, M.R. Daymond, L. Edwards, J.A. James, J.R. Santisteban, Phys. B: Condens. Matter 350 (2004) E511–E514.
[23] R.A. Young, Rietveld Method, Oxford University Press, Oxford, 1993.
[24] R. Hill, The Mathematical Theory of Plasticity, Clarendon Press, Oxford Classic Series, 1998, p. 26.
[25] M.P. Jackson, R.C. Reed, Mater. Sci. Eng. A 259 (1999) 85–97.

[26] J. Mao, K.-M. Chang, W. Yang, D.U. Furrer, K. Ray, S.P. Vaze, Mater. Sci. Eng. A 332 (2002) 318–329.
[27] F. Torster, G. Baumeister, J. Albrecht, G. Lütjering, D. Helm, M.A. Daeubler, Mater. Sci. Eng. A 234–236 (1997) 189–192.
[28] R. Cozar, A. Pineau, Metall. Trans. 4 (1973) 47–59.
[29] L. Wang, M. Preuss, P.J. Withers, G.J. Baxter, P. Wilson, Metall. Mater. Trans. B 36 (2005) 513–523.
[30] J. Bouchard, P.J. Withers, J. Neutron Res. 12 (2004) 81–91.
[31] Personal Communication with Dr. M. Hardy, Dr. J. Orr, Rolls-Royce plc., 2005.